SUPPLEMENTARY INFORMATION

Single-molecule mid-IR detection through vibrationally-assisted luminescence

Rohit Chikkaraddy*[1], Rakesh Arul[1], Lukas A. Jakob[1], and Jeremy J. Baumberg*[1]

[1] NanoPhotonics Centre, Cavendish Laboratory, Department of Physics, JJ Thompson Avenue, University of Cambridge, Cambridge, CB3 0HE, United Kingdom

Contents

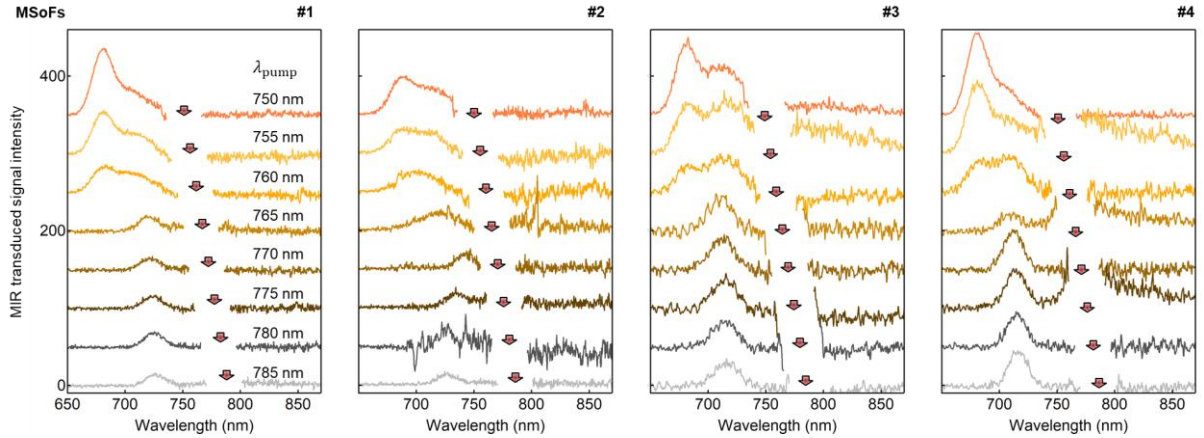

Figure S1: MIR vibrationally-assisted luminescence (MIR-VAL) in additional samples. (**a**) Pump wavelength dependent MIR-VAL for CB-MB system in four different microsphere-on-foil (MSoF) cavities.

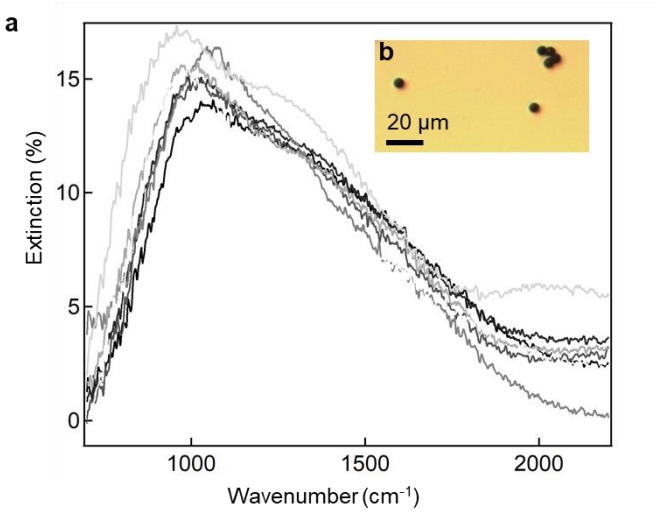

Figure S2: Fourier transform infrared (FTIR) spectroscopy of individual MSoF cavities. (**a**) Mid-infrared extinction spectra obtained for different MSoF cavities. (**b**) Bright field optical image of several isolated MSoF constructs.

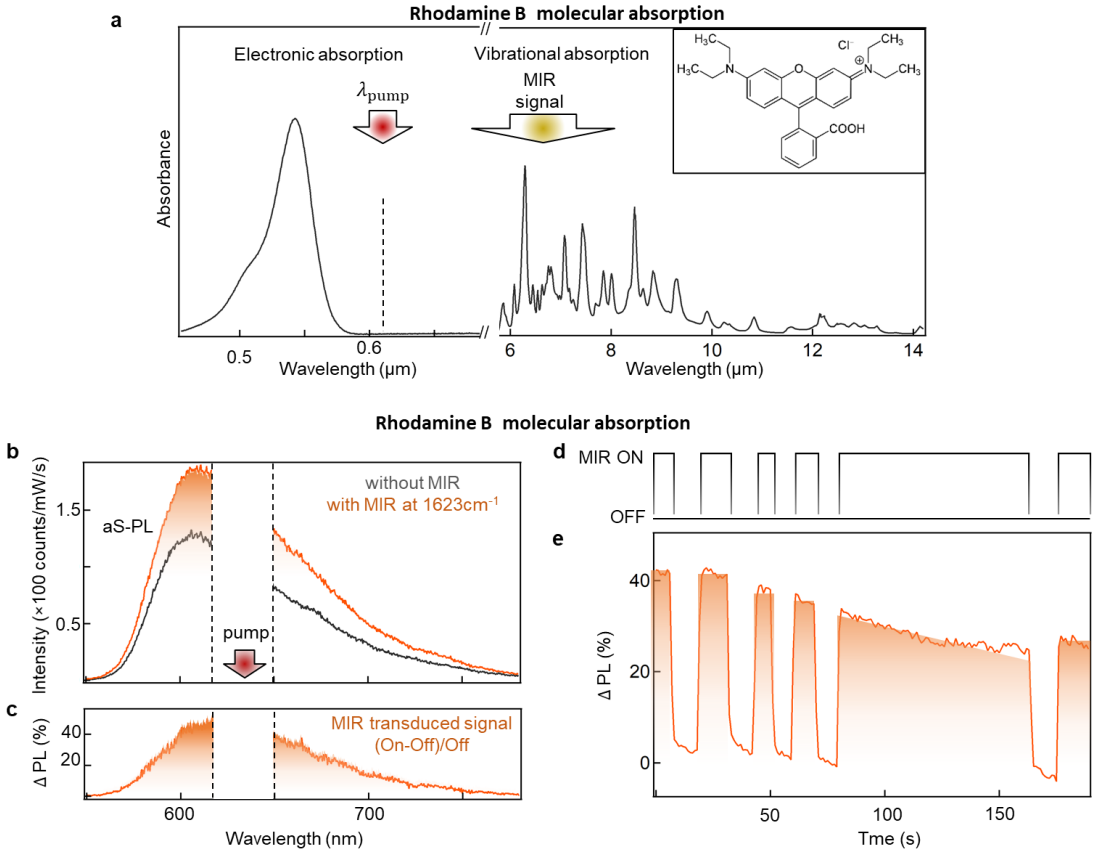

Figure S3: Detecting MIR-VAL in rhodamine B (RhB) molecules. (**a**) Electronic and vibrational absorption spectra of RhB molecules in solution. Arrows indicate NIR and MIR tuning. Inset shows the chemical structure of RhB. The assembly of RhB into the MSoF cavity is obtained using supramolecular assembly inside a cucurbit[7]uril (CB[7]) host molecule. (**b**) Stokes and anti-Stokes emission from pump ($\lambda_{\mathrm{pump}} = 633\mathrm{nm}$), with (orange) and without (grey) MIR light of average power 0.5μW/μm^2 on a single MSoF cavity. (**c**) Percentage difference in emitted signal transducted by MIR. (**d,e**) Modulation of (e) aS-PL intensity while switching the (d) MIR beam on and off.

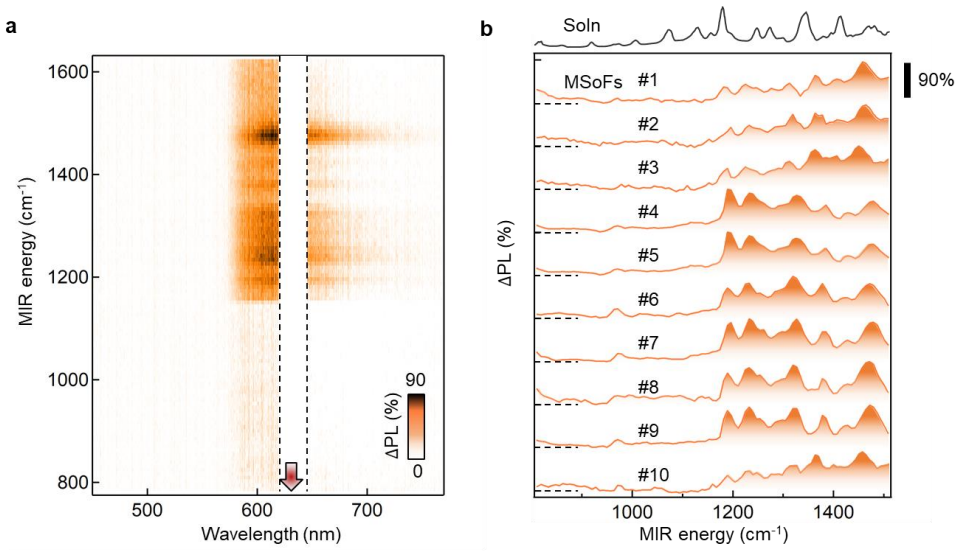

Figure S4: MIR spectrally-tuned vibrationally-assisted luminescence for RhB. (**a**) aS-PL intensity when tuning MIR energy on a single MSoF nanocavity. (**b**) Series of MIR-VAL spectra obtained for different MSoF cavities (#1 to #10) and compared to FTIR measurements of RhB in solution (solid grey line, top).

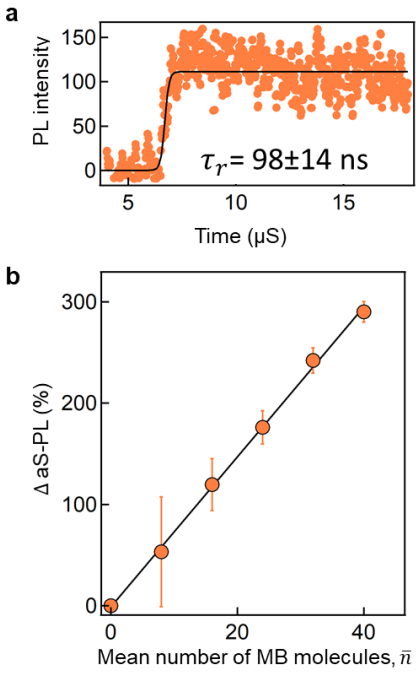

Figure S5: Temporal and spatial coherence of MIR-VAL. (**a**) Measured rise of aS-PL intensity on illuminating the individual MSoF cavity with QCL laser pulses, using single-photon detection. The experimental data is fit with a sigmodal curve to extract the rise time (τ_r). (**b**) Variation in aS-PL intensity when varying the mean number of MB molecules in individual MSoF cavities, across different samples. Error bars show standard deviation of as-PL on >10 MSoFs.

Section S1: Rate Equation Model

The population dynamics of the MIR-VAL process is modelled using rate equations involving four states (Eqs.S1-S4), as shown in Fig.S6 (and Fig.1b in the main text). The ground state $|0\rangle$ population N_0 is coherently driven to the first vibrational state $|1_a\rangle$ by MIR light tuned to their energy difference. The population (N_{1a}) of $|1_a\rangle$ is defined by the rate of MIR light absorption, which in turn depends on the MIR photon flux (ϕ_{MIR}) and absorption cross-section (σ_{MIR}). This σ_{MIR} is modified by the presence of the nanocavity, which is accounted for by the near-field intensity enhancement $(E^2/E_0^2)_{MIR}$ estimated from full-wave simulations (Fig.1f). The vibrationally populated states relax back to $|0\rangle$ at rates which are well characterised and ~1ps for these molecules at room temperature [14,15 in main text]. The proximity of metals is known to speed up vibrational relaxation but remains on the ps scale.

The transition from $|0\rangle$ to $|0'\rangle$ is similarly driven by the pump beam, with population dynamics at state $|0'\rangle$ (coherent population $N_0^{'c}$) governed by the pump flux (ϕ_{pump}), cross-section at pump wavelength (σ_{pump}), as well as its near-field intensity enhancement $(E^2/E_0^2)_{\mathrm{pump}}$. In all dye molecules, there is then rapid small-energy relaxation from the initially electronically-excited state due to intramolecular rotations and vibrations (ivr). This population N_0^c thus loses its coherence, relaxing to the slightly lower energy state $|0'\rangle$ at rate γ_{ivr} which is on the order of (100fs)$^{-1}$. The vibrationally relaxed state (N_0') ultimately emits aS-PL to radiative relax back to $|0\rangle$. This rate of relaxation from $|0'\rangle$ to $|0\rangle$ (γ_r) is enhanced by the Purcell factor (P) of the nanocavity. The estimated values of pumping, Purcell and decay rates are tabulated in Fig. S6c. The optical cross-section of electronic and vibrational transitions of molecule outside the nanocavity are σ_{Pump}=10^{-3}nm^2 and σ_{MIR}=10^{-5}nm^2, respectively. The rate equations then follow:

$$\frac{\partial N_0}{\partial t} = -\phi_{MIR}\,\sigma_{MIR}\left(\frac{E^2}{E_0^2}\right)_{MIR}(N_0 - N_{1a}) + N_{1a}/\gamma_v + N_0^{'}/(P.\gamma_r) \tag{S1}$$

$$\frac{\partial N_{1a}}{\partial t} = \phi_{MIR}\,\sigma_{MIR}\left(\frac{E^2}{E_0^2}\right)_{MIR}(N_0 - N_{1a}) - \phi_{\mathrm{pump}}\sigma_{\mathrm{pump}}\left(\frac{E^2}{E_0^2}\right)_{\mathrm{pump}}(N_{1a} - N_0^c) - N_{1a}/\gamma_v \tag{S2}$$

$$\frac{\partial N_0^c}{\partial t} = \phi_{\mathrm{pump}}\sigma_{\mathrm{pump}}\left(\frac{E^2}{E_0^2}\right)_{\mathrm{pump}}(N_{1a} - N_0^c) - \frac{N_0^c}{\gamma_{ivr}} \tag{S3}$$

$$\frac{\partial N_0'}{\partial t} = \frac{N_0^c}{\gamma_{ivr}} - \frac{N_0'}{P.\ \gamma_r} \tag{S4}$$

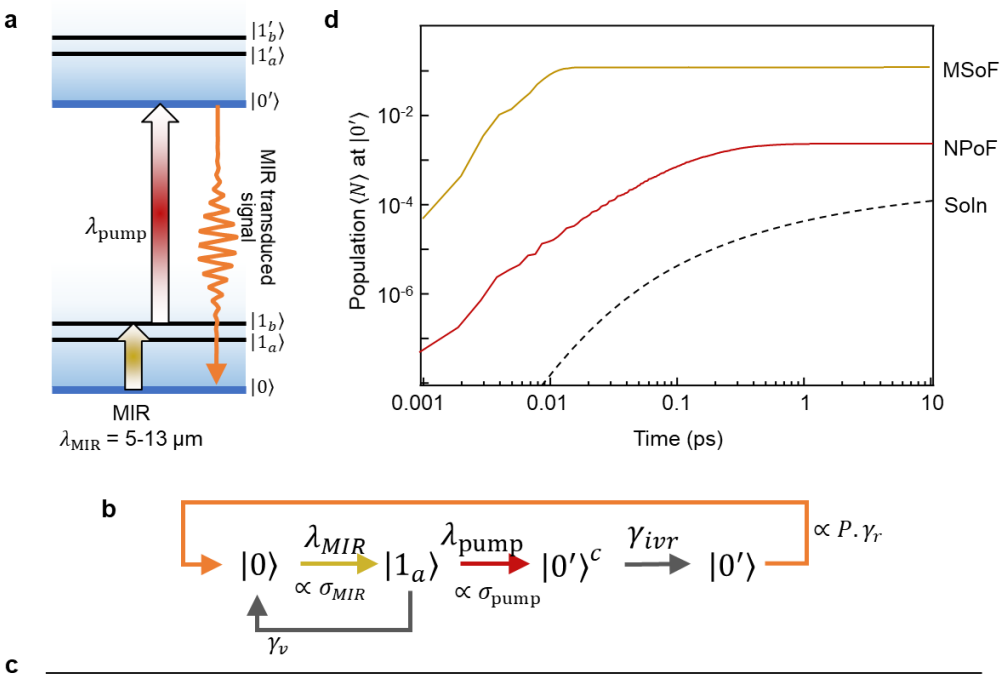

c

	$\left(\frac{E^2}{E_0^2}\right)_{MIR}\sigma_{MIR}$ (nm^2)	$\left(\frac{E^2}{E_0^2}\right)_{\text{pump}}\sigma_{pump}$ (nm^2)	$1/\gamma_v$ (ps)	$1/\gamma_{ivr}$ (ps)	$1/(P.\gamma_r)$ (ps)
Solution	10^{-5}	10^{-3}	1..0	0.1	1000
MSoF	$10^5\times10^{-5}$	$10^4\times10^{-3}$	1.0	0.1	10
NPoF	$10^2\times10^{-5}$	$10^5\times10^{-3}$	1.0	0.1	1.0

Figure S6: Temporal dynamics of MIR-VAL. (**a**) Energy diagram of electronic and vibrational levels of molecular dyes involved in the MIR-VAL process. (**b**) Modelling of energy states as a four-level system with rates of transition governed by differential equations described in the text. (**c**) Table of parameters used to describe the transitions. (**d**) Estimated population $\langle N_0^{'} \rangle$ at $|0'\rangle$ involved in aS-PL emission for the different nanocavity systems studied.

Section S2: Measurement of MIR-VAL efficiency

To first directly measure the transduction efficiency without confusion with coupling efficiencies, we compare the measured aS-PL under MIR pumping with the molecular PL intensity when directly pumping the same MSoF cavity using the same collection system on the same device (Fig.2e). This is achieved by tuning to a pump wavelength λ_{pump}=633nm which drives the $|0\rangle \rightarrow |0'\rangle$ transition without MIR light. The light emission from each MSoF cavity at λ_{pump}=633nm is compared with transducting $\lambda_{\mathrm{pump=750nm}} + \lambda_{\mathrm{MIR}}$ at the same power density. In this way we find the direct efficiency of MIR-VAL to be >10%. Since we do not yet see saturation with MIR power, it seems that at higher MIR powers (unattainable in the current experiment) the transducted signal could equal that pumped directly with the same pump power.

To estimate the absolute MIR transduction efficiency, we directly compare the integrated aS-PL counts with the number of MIR photons illuminated on the sample.

The number of MIR photons illuminated n_{MIR}=$P_{MIR} \times \lambda_{\mathrm{MIR}}/hc$, where P_{MIR} is the MIR power, h is Planck's constant and c is the speed of light. The estimated n_{MIR} with 1mW average power at λ_{MIR}=6.3μm is 3.2×10^{16}. However, a large fraction of MIR light is reflected from the foil and the MIR transmission of the 10nm Au foil is 10^{-4}. Therefore, the number of MIR photons illuminating each MSoF cavity is 3.2×10^{12}.

We calibrate the detection efficiency of our system at λ_{pump} by measuring the reflected light from the Au foil beside the MSoF cavity. After accounting for losses due to the objective lens, beam splitters (90:10 and 30:70), mirrors (7) and monochromator, the overall efficiency of detection is ~10%. Note that not all the light scattered from the MSoF cavity is collected by the objective lens - the nanocavity system is known to emit as a vertical dipole with angular cone larger than the NA of collection lens which limits the collection efficiency to 10^{-2} [22,24].

Comparing now with the measured aS-PL photon counts at 1mW of MIR power of 3×10^4 (Fig. 3b), which gives an estimated end-to-end MIR transduction of 10^{-6} currently. We note that improved coupling efficiencies using resonant MIR antennas (as in [15]) without the opaque foil will greatly improve this (by $>10^5$). Also importantly, λ_{pump} used to transduce the MIR signal is not operating near the saturation limit of molecular light emission, which indicates that higher pump powers will further improve the transduction efficiency.